

Article

Microstructural Characterization and Mechanical Properties of Direct Quenched and Partitioned High-Aluminum and High-Silicon Steels

Pekka Kantanen *, Mahesh Somani, Antti Kaijalainen , Oskari Haiko, David Porter and Jukka Kömi

Materials and Mechanical Engineering, Centre for Advanced Steels Research, University of Oulu, P.O. Box 4200, FI-90014, 90570 Oulu, Finland; mahesh.somani@oulu.fi (M.S.); antti.kaijalainen@oulu.fi (A.K.); oskari.haiko@oulu.fi (O.H.); david.porter@oulu.fi (D.P.); jukka.komi@oulu.fi (J.K.)

* Correspondence: pekka.kantanen@oulu.fi

Received: 4 February 2019; Accepted: 18 February 2019; Published: 21 February 2019



Abstract: A new experimental steel containing in weight percent 0.3C-2.0Mn-0.5Si-1.0Al-2.2Cr and 0.3C-1.9Mn-1.0Si-1.0Cr was hot rolled in a laboratory rolling mill and directly quenched within the martensite start and finish temperature range. It was then partitioned without reheating during slow furnace cooling to achieve tensile yield strengths over 1100 MPa with good combinations of strength, ductility and impact toughness. Gleeble thermomechanical simulations led to the selection of the partitioning at the temperatures 175 and 225 °C, which produced the desired microstructures of lath martensite with finely divided retained austenite in fractions of 6.5% and 10% respectively. The microstructures were analyzed using light and scanning electron microscopy in combination with electron backscatter diffraction and X-ray diffraction analysis. The mechanical properties were characterized extensively using hardness, tensile and Charpy V impact testing. In tensile testing a transformation induced plasticity mechanism was shown to operate with the less stable, carbon-poorer retained austenite, which transformed to martensite during straining. The auspicious results in respect to microstructures and mechanical properties indicate that there are possibilities for developing tough ductile structural steels through thermomechanical rolling followed by the direct quenching and partitioning route.

Keywords: direct quenching and partitioning; thermomechanical rolling; advanced high strength steels; retained austenite; martensite

1. Introduction

There has been an ever-growing need to develop advanced high strength steels (AHSS) with better combinations of mechanical properties such as high strength, ductility, toughness and formability. To meet these growing challenges, new optimal designs of inexpensive compositions and/or thermomechanical processing (TMP) routes must be continuously developed. Typically, quenching and tempering is used to obtain high strength and good impact toughness for structural steels [1,2]. In uniaxial tensile testing at room temperature, the ductility of these steels in terms of their reduction of area to fracture or elongation is generally acceptable. However, their uniform elongation and work hardening capacity is moderately low [2]. This can restrain the wider application of these steels, as strain localization during manufacturing or overloading in service can impair the integrity of the structure [2].

Speer et al. [3] described the constrained paraequilibrium (CPE) model and proposed a new quenching and partitioning (QP) process which resulted in mixtures of martensite and austenite

microstructures. QP processing includes austenitization annealing, quenching to a temperature between the martensite start (M_s) and finish (M_f) temperatures and holding at the quenching stop or adequate higher temperatures for a certain duration in order to facilitate the partitioning of carbon from supersaturated martensite to austenite. Austenite can thereby be partially or fully stabilized down to room temperature or even lower [3,4]. Alloying with Si, Al or P is intentionally used to hinder the formation of iron carbides and the decomposition of austenite. As Thomas et al. [5] described, while the martensitic matrix provides the required high strength, the presence of a small fraction of austenite finely divided between the martensite laths improves work hardening and uniform elongation through a transformation induced plasticity (TRIP) effect. Large volume fractions of austenite enable the achievement of a good combination of strength and ductility without the use of expensive alloying elements. For instance, Arlazarov et al. [6] analyzed true stress–true strain curves together with the work hardening rate (WHR) as a function of strain and demonstrated that extremely high strength steels with adequate ductility can be obtained using QP treatment. In recent years, QP has shown huge potential in offering interesting mixtures of strength, ductility and toughness in ultra-high strength steels, particularly in respect to low temperature impact toughness, in addition to uniform and total elongation and work hardening capacity [3,5–8].

Si is the element most commonly used to prevent carbide precipitation in QP steels. There is relatively little published regarding the use of Al. Al alloyed steels could be encouraging candidates for use in continuous galvanizing processes due to their lower Si contents. Si can form adherent oxides, which detrimentally effect zinc coating wettability and surface quality [9,10]. De Moor et al. [11] showed that at a given carbon level of 0.25% a higher volume fraction of retained austenite (RA) was obtained for CMnSi steel (Si 1.45% and Al 0.3%) than for CMnSiAl steel (Si 0.55% and Al 0.69%), indicating that Al might be less effective than Si in retarding the formation of transition carbides. In yet another investigation, Tsukatani et al. [12] hot rolled and isothermally processed 0.2% carbon steels with Mn and Si with contents varying in the range 1.0%–2.0%. After isothermal holding at 400 °C for 30 min, a maximum retained austenite volume fraction of 20.2% was obtained in steel containing 2.0% Si and 1.5% Mn in a bainitic–martensitic microstructure. A reduction in the finish rolling temperature (FRT) close to the ferrite start temperature (A_{r3}) was shown to raise the volume fraction of RA. Also when lower C content was considered (down to 0.15%), Si was shown to be more efficient than Al in retarding transition carbide formation [13].

The present study focuses on the evaluation of the microstructures and mechanical properties of two 0.3C steels containing either high silicon or high aluminum contents, which were processed via thermomechanical rolling followed by direct quenching and partitioning (TMR-DQP), as proposed by Somani et al. [8]. Previously, Somani et al. [8,14] reported that such processing applied to 0.2C steels could produce a yield strength of about 1100 MPa combined with adequate ductility, good low-temperature and upper shelf toughness, and a hardness close to that expected of a fully martensitic structure. In the literature, there were only a few papers dealing with the direct quenching and partitioning (DQP) process, despite their promising strength and ductility combinations. In addition to Tsukatani et al. [12], Thomas et al. [5], Somani et al. [8], Li et al. [15] and Tan et al. [16] described DQP-type processes. The treatment presented by Tsukatani et al. [12] is not a DQP process but is very similar. Thomas et al. [5] proposed a DQP rolling process based on Gleeble thermal simulations, but no actual rolling treatments were studied. Li et al. [15] and Tan et al. [16] used different rolling schedules, cooling rates, quenching stop temperatures (TQ) and coiling times compared to those used in the current TMR-DQP process. In the present study actual laboratory hot rolling experiments were conducted. The specific aim of this work was to establish a DQP route to achieve a yield strength over 1100 MPa combined with improved ductility and low temperature impact toughness. The approach used involved choosing prospective chemical compositions with higher carbon content (0.3%) and inexpensive alloying, finding applicable DQP processing parameters, with the aid of physical simulation on a Gleeble 3800, and, finally, testing and evaluating the DQP materials after processing on a laboratory rolling mill.

2. Materials and Methods

The two experimental steels shown in Table 1 were vacuum cast as 100 kg ingots, which were cut into two halves along the centerline in order to circumvent the problem of centerline segregation that may adversely influence and cause scatter in mechanical properties. These materials were used for preliminary physical simulation experiments on a Gleeble 3800 and for direct quenching and partitioning experiments on a laboratory hot rolling mill.

Table 1. Chemical compositions (wt%) of experimental steels.

Material	C	Si	Mn	Al	Cr	N	S	P
Steel A	0.30	0.56	2.00	1.10	2.20	0.0010	0.0010	0.0010
Steel B	0.30	0.99	1.86	0.01	1.01	0.0031	0.0009	0.0026

Contact dilatation measurements on a Gleeble 3800 thermomechanical simulator (Dynamic Systems Inc., Poestenkill, NY, USA) suggested that partitioning temperatures of 175 and 225 °C would be appropriate for obtaining initial martensite fractions at the partitioning temperature in the range 85%–95%.

TMR-DQP experiments were conducted on both steels on a two-high, reversing laboratory rolling mill with blocks of $120 \times 80 \times 60 \text{ mm}^3$ cut from the cast ingots. The blocks were heated at 1200 °C for 2 h in a furnace prior to the two-stage rolling resulting in 12 mm thick plates. During rolling and quenching, the temperature was continuously measured with thermocouples placed in holes drilled on the longitudinal sides of the samples, mid-width and mid-length. Four controlled recrystallization rolling passes, of about 0.2 strain each, were performed above 1030 °C, followed by four passes, of about 0.2 strain each, below approximately 900 °C in the non-recrystallization temperature regime. Directly after rolling the samples were quenched in a water tank and held there until the temperature reached the desired quench stop temperature (T_Q), i.e., 175 or 225 °C (± 10 °C), after which they were transferred to a furnace and preheated to the same quench stop temperature. After transferring the rolled and quenched plates, the furnace was switched off to enable a slow cooling, over 50 h, to room temperature (RT) in order to simulate the coiled strips cooling in actual industrial rolling. The TMR-DQP schedules are given in Figure 1. In addition, one sample of both of the steels was thermomechanically rolled in the manner described above, followed by direct quenching to room temperature (TMR-DQ), in order to be able to compare the flow stress behavior, microstructures and mechanical properties obtained via TMR-DQP processing with TMR-DQ processing.

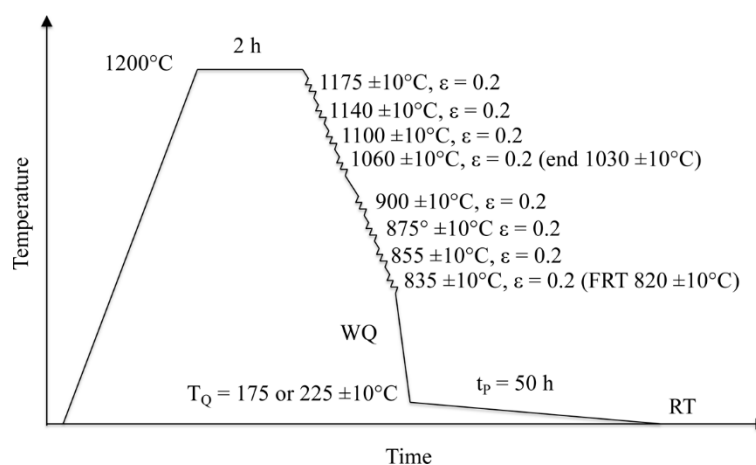


Figure 1. Hot rolling and partitioning schedule.

The volume fraction of the retained austenite to room temperature and its mean carbon content (C_γ) were determined using X-ray diffraction (XRD) in a Rigaku SmartLab 9 kW XRD (Rigaku

Corporation, Tokyo, Japan) unit with a Co anode and PDXL2 analysis software (PDXL 2.6.1.2, Rigaku Corporation, Tokyo, Japan). In the XRD measurements, a de-texturing method was used, i.e., the samples were tilted (χ) with 10° steps from 0 to 60° and rotated (Φ) 360° during measurements to eliminate any possible effects of the steel sample texture on the measurements. A Rietveld refinement technique was used in the determination of the residual austenite lattice parameter (a_γ). The average room temperature carbon contents in the RA were estimated based on the lattice parameter measurements using the following equation described by Dyson and Holmes [17] and Van Dijk et al. [18]:

$$a_\gamma = 3.556 + 0.0453x_C + 0.00095x_{Mn} + 0.0056x_{Al} + 0.0006x_{Cr}, \quad (1)$$

where a_γ is the austenite lattice parameter (\AA) and x_C , x_{Mn} , x_{Al} and x_{Cr} are the concentrations of carbon, manganese, aluminum and chromium, respectively, in wt%. Dyson and Holmes [17] showed that the influence of silicon on the lattice parameter of austenite was negligible. According to Scott and Drillet [19], a comparison of the average value of C_γ obtained from electron energy loss spectroscopy (EELS) data, with austenite lattice parameters obtained using XRD, showed a nonlinear relationship, which may have been the result of varying stress states in the RA. This makes it complicated to define the most appropriate equation relating a_γ to C_γ .

Tensile test specimens with a size of $\Phi 6$ mm (d), 80 mm overall length (L_f), 40 mm length of reduced section (L_c) and a gauge length of 30 mm (L_0) were machined according to the standard SFS-EN ISO 6892-1, with the axis of the bar transverse to the rolling direction in the rolling plane. Tensile and interrupted tensile tests were carried out in a Zwick Roell Z100 100 kN tensile testing machine (ZwickRoell GmbH & Co., Ulm, Germany) in order to determine the flow stress and work hardening behaviors. In order to evaluate the impact toughness of the DQP processed samples at different temperatures, $10 \times 10 \times 55$ mm³ Charpy V notched specimens were machined according to the standard EN 10045-1 with the axis of the bar parallel to the rolling direction in the rolling plane, i.e., longitudinal specimens. For hardness evaluation, Vickers hardness measurements were made using a HV10 load on a Struers Duramin A-300 (Struers A/S, Ballerup, Denmark) with sections containing the L-T, L-N and T-N directions, where L is the longitudinal (rolling) direction, T is the transverse direction and N is the direction of the normal to the rolled plate. The L-T section was cut at the quarter-thickness depth.

General microstructural characterization was done using Nikon Eclipse MA100 light optical microscopy (LOM) (Nikon Corporation, Kanagawa, Japan) and field emission scanning electron microscopy (FESEM) (Carl Zeiss AG, Oberkochen, Germany). LOM samples were polished and etched with 2% nital. FESEM samples for electron backscatter diffraction (EBSD) were polished using silica suspension (0.04 micron) during the final step according to standard procedure. Microstructural characterizations were done at the quarter-thickness position on L-T and L-N sections. The linear intercept (LI) method, applied to specimens etched with a mixture of picric acid (1.4 g), distilled water (100 mL), Agepol (1 mL) and HCl (4–5 drops), was used to determine the prior austenite grain size (PAGS) on L-N sections using LOM.

To determine the microtexture and the division of austenite in the martensitic lath structure, EBSD measurements were made for all the TMR-DQP samples. Lath structure and austenite pool were measured using a Zeiss Sigma FESEM EBSD (Carl Zeiss AG, Oberkochen, Germany) with EDAX-OIM acquisition and analysis software (7.1.0, Ametek Inc., Berwyn, PA, USA). The step size was 40 nm. A Zeiss Ultra Plus FESEM-EBSD (Carl Zeiss AG, Oberkochen, Germany) was used to record texture data, using Oxford HKL acquisition and analysis software (HKL Channel5 5.12.56.0, Oxford HKL, London, UK). A step size of 0.20 μm was used for texture measurements.

3. Results and Discussion

3.1. Determination of M_s Temperature

Figure 2a,b shows the typical dilatation behavior of a QP sample for steel A and B. During dilatation measurement in the Gleeble simulator the sample was soaked at 1150 °C, followed by cooling to the deformation temperature, 800 °C. It was deformed with three hits of approximately 0.2 strain each at a strain rate of 1 s⁻¹. After deformation, the sample was cooled at 30 °C/s to a quenching and partitioning temperature of 200 °C. After a 3000 s partitioning time (t_p), the sample was air cooled to room temperature. Figure 2 shows that martensite formation started close to 325 °C for both steels. During partitioning, a small fraction of austenite can decompose to bainite producing the step in the dilatation curve at 200 °C as shown by the arrow in Figure 2. Some secondary martensite can form during final cooling to RT (as shown by the arrow at 100 °C). However, as shown below, most of the austenite enriched with carbon can be retained at room temperature.

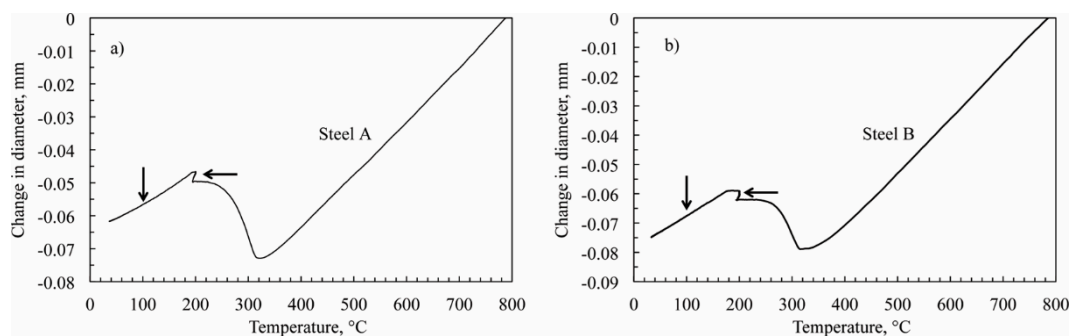


Figure 2. A dilatation curve for steel A (a) and steel B (b).

3.2. Retained Austenite of Hot-Rolled and Partitioned Materials

The targeted martensite phase fractions at the chosen quench stop temperatures (T_Q) were in the ranges of 85%–90% and 90%–95%. The volume fractions of martensite (V_M) at a given T_Q can be estimated from the Koistinen and Marburger (KM) equation [20]:

$$V_M = 1 - \exp(-\alpha_m(T_{KM} - T_Q)), \quad (2)$$

where, α_m is a composition-dependent rate parameter and T_{KM} is the so-called theoretical martensite start temperature, as proposed by van Bohemen and Sietsma [21]. The composition dependence of the rate parameter α_m was described by the following equation, as given below using the equation of van Bohemen and Sietsma [21]:

$$\alpha_m = 0.0224 - 0.0107x_C - 0.0007x_{Mn} - 0.00005x_{Ni} - 0.00012x_{Cr} - 0.0001x_{Mo}, \quad (3)$$

where the concentration x is in wt%. Using M_s temperatures as 325 °C, estimated from dilatation measurements, the calculated values of V_M according to Equations (2) and (3) for the two steels are about 93% and 83% martensite corresponding to the T_Q temperatures of 175 and 225 °C, respectively.

Figure 3 shows the room temperature volume fractions of RA measured at the 1/4 thickness (on L-T faces) of the hot-rolled and partitioned specimens and the corresponding mean values of bulk hardness (HV10) plotted against T_Q . As expected, hardness decreased as a consequence of the increase in the amount of retained austenite and the hardness was higher with the DQP treated steel B than with steel A. A detailed discussion on hardness data will be presented later in connection with the tensile properties. A high fraction of RA, ca. 10% was obtained for both steels after DQP processing with $T_Q = 225$ °C in comparison with about 6% RA with $T_Q = 175$ °C. The fraction of RA in steel A (Al alloyed) was at the same level as that of steel B (Si alloyed), although Al might be less effective than Si

in retarding the formation of transition carbides. This is probably the result of the higher combined content of Si and Al (1.66%) in steel A compared to the Si content (0.99%) in steel B. The average carbon contents for $T_Q = 225\text{ }^\circ\text{C}$ were determined to be 0.65% and 0.94% respectively for steels A and B. In comparison, at $T_Q = 175\text{ }^\circ\text{C}$, the average carbon content in the retained austenite of steels A and B were determined to be 0.60% and 0.61%, respectively. According to the constrained paraequilibrium (CPE) model described by Speer et al. [3], the carbon concentration in austenite should decrease with increasing T_Q . However, the carbon content in the retained austenite of the DQP processed specimens showed a marginal increase with increasing T_Q from 175 to 225 $^\circ\text{C}$. On the other hand, at the lower T_Q ($= 175\text{ }^\circ\text{C}$), a higher fraction of martensite holds more supersaturated carbon due to the lower fraction of RA, but the diffusion rate can be too low at this temperature to equilibrate a higher carbon content in the RA. De Moor et al. [22] reported that for QP processed 0.3C-3Mn-1.6Si steels, up to 15.4% RA contents containing an average of 1% C were obtained with the moderately short partitioning times (t_p) of 30 and 100 s ($T_Q = 180\text{--}220\text{ }^\circ\text{C}$ and $T_p = 400\text{ }^\circ\text{C}$). However, an increase in t_p , over 30–100 s, resulted in a reduced fraction of RA. Maheswari et al. [23] reported a RA fraction of about 16% for a 0.29C-1.22Mn-1.65Si-1.62Al QP processed steel. Through QP processing, higher RA contents have been achieved because there is a possibility to use low T_Q temperatures combined with higher t_p times. By utilizing the TMR-DQP process, it is possible to reach moderate to high RA, even though sluggish carbon diffusion at low T_Q can restrict the RA fraction.

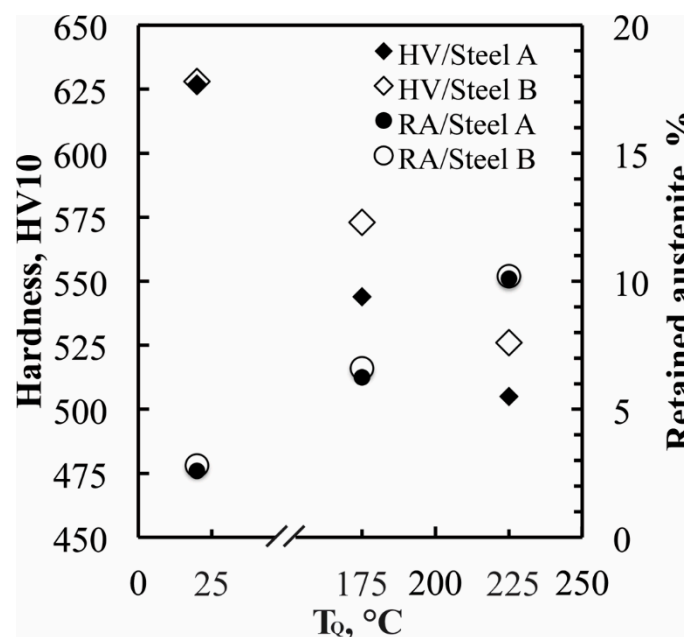


Figure 3. Effect of quench stop temperature (T_Q) on HV10 hardness and volume fraction of retained austenite (RA) in laboratory hot-rolled samples via thermomechanical rolling followed by direct quenching and partitioning (TMR-DQP) process.

3.3. Microstructural Characterization

Preliminary LOM microstructural characterization showed that the overall microstructures of both investigated hot-rolled and partitioned materials, irrespective of T_Q (i.e., 175 and 225 $^\circ\text{C}$), was lath martensite. A more detailed microstructure characterization was done using FESEM-EBSD, although the interlath RA was very difficult to resolve using this technique as it is too finely divided between martensitic laths in comparison with the EBSD resolution limit (about 0.1–0.2 μm). In spite of the Si and Al alloying, both investigated steels revealed the occurrence of precipitation for both quench stop temperatures, i.e., 175 and 225 $^\circ\text{C}$, as shown in Figure 4. As Edmonds et al. [24] depicted delayed cementite precipitation by alloying to Si, these precipitates are probably transition ϵ -carbides. They

were also observed in the DQ samples, suggesting that they might have formed during the quenching itself. Edmonds et al. [24] described that Si has a high solubility in ϵ -carbide and may facilitate its formation. Increasing Si content can, therefore, stabilize transition carbide at lower quenching temperatures. Edmonds et al. [24] showed that Si has a low solubility in cementite and is known to retard its formation. Figure 4 illustrates that the microstructures of both steels, as seen in FESEM images, are very similar whether $T_Q = 175$ or 225 °C. Carbide precipitates were more perceptible with the higher T_Q .

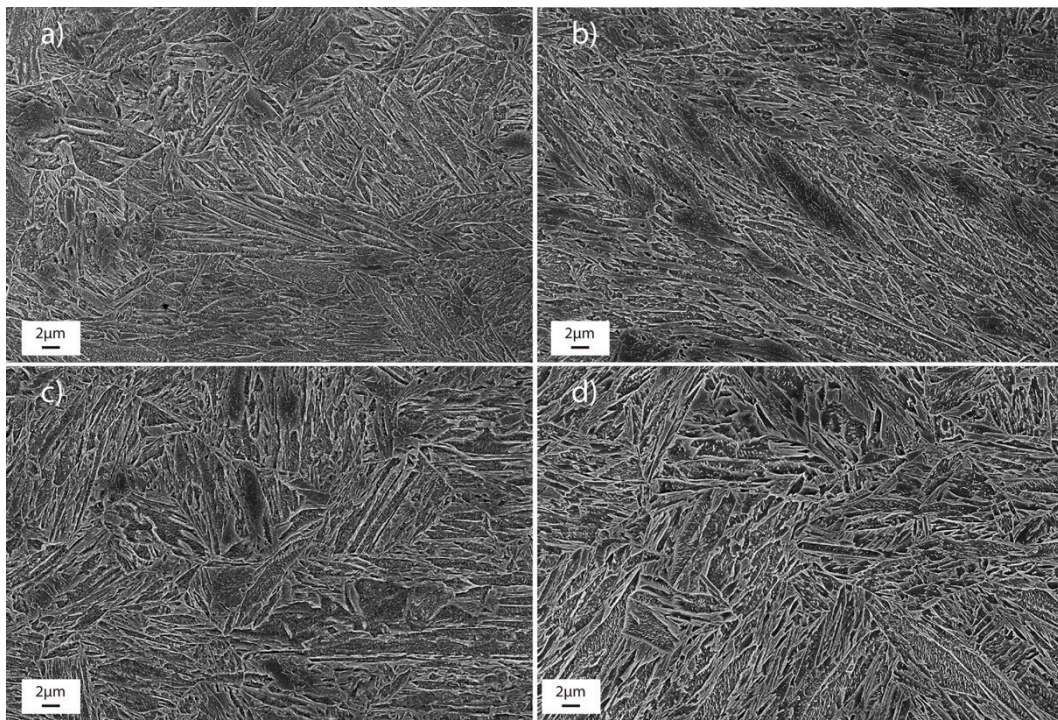


Figure 4. Field emission scanning electron microscopy (FESEM) micrographs of the martensitic structure of hot-rolled TMR-DQP specimens. Steel A, (a) $T_Q = 175$ °C and (b) $T_Q = 225$ °C; and steel B, (c) $T_Q = 175$ °C and (d) $T_Q = 225$ °C.

Using EBSD, some tiny pools of RA, about 0.5–1 μm in diameter, with a volume fraction less than 1% could be identified, as shown in Figure 5, but thin interlath RA was not detected for the reason stated above. For the TMR-DQP processed steels with $T_Q = 225$ °C, EBSD scans with a step size of 40 nm gave RA volume fractions of only 0.8 and 0.6% for steels A and B, respectively. Comparing these RA values to those determined by XRD, i.e., volume fraction circa 10%, suggests that more than 90% of the RA is finely divided as films between the martensite laths and less than 10% as pools resolvable in EBSD images. The formation of RA pools can be partially due to compositional differences caused by interdendritic segregation during casting, which are only slightly reduced by ingot soaking before the TMR-DQP processing [14]. The austenite pools are smaller than the width of the segregation lines in the TMR-DQP processed samples.

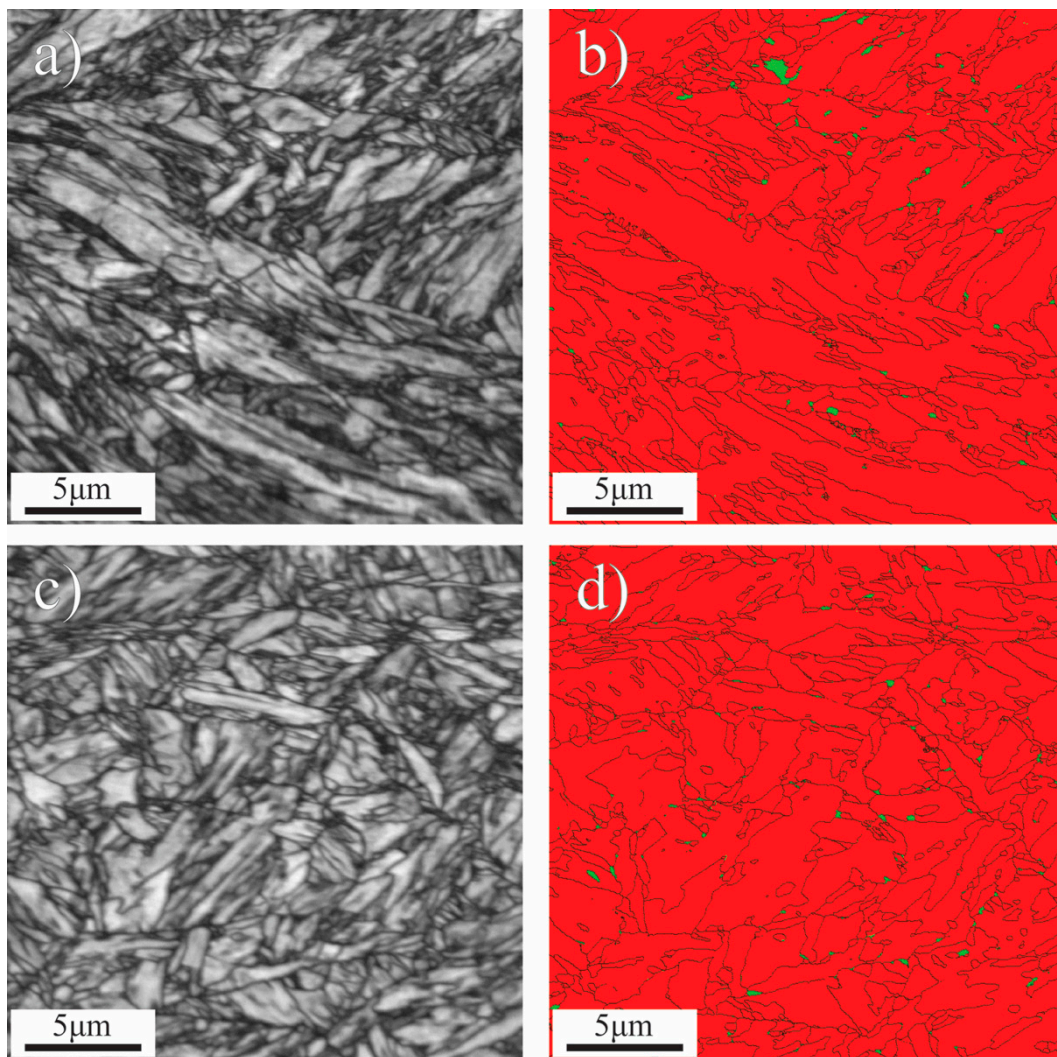


Figure 5. Micrographs showing electron backscatter diffraction (EBSD) image quality (IQ) maps and high-angle grain boundaries (step size 40 nm) for steel A (a,b) and for steel B (c,d) at $T_Q = 225$ °C. In the colored images green is austenite.

Texture analysis was performed using EBSD data and indicated low texture intensity. The highest texture peaks, 4.2 for $\{112\}\langle 110\rangle$ and 2.8 for $\{554\}\langle 225\rangle$, were observed for DQP processed steel A with $T_Q = 175$ °C. In comparison, Kaijalainen et al. [25] observed texture intensities of 6 for $\{112\}\langle 110\rangle$ and 7 for $\{554\}\langle 225\rangle$ for a pilot-scale hot rolled C-Si-Mn-Cr-Ti-B ultra-high strength strip steel.

The mean linear intercept (MLI) method was used to determine PAGS on L-N planes parallel to the rolling (L) and normal directions (N) using LOM. It should be noted, however, that prior austenite grain boundaries were difficult to etch due to the high purity, i.e., low P content, of the steels, so the values are only approximate. It can be seen that pancaking was negligible i.e., grain aspect ratios were low (1.26–1.50) despite the fact that four passes of 0.2 strain each were applied in the temperature regime 900–835 °C. In comparison, Hannula et al. [26] reported an aspect ratio of up to 3.5 for low-carbon steel subjected to laboratory rolling. The low aspect ratios imply that recrystallization occurred even during the controlled rolling at or below 900 °C.

The EBSD data enabled the determination of mean lath size (d_1), mean effective grain size (d) and effective grain size at 90% in the cumulative size distribution ($d_{90\%}$) using equivalent circle diameter (ECD) values as the measure of size. d and d_1 were determined as ECD values with high-angle ($>15^\circ$) and low-angle ($2.5\text{--}15^\circ$) boundary misorientations, respectively. These values together with $d_{90\%}$ and

PAGS are shown in Table 2. The PAGS values were at the same level for both steels. d_1 and d values were also at the same level except for steel B, with $T_Q = 175$ °C, which had smaller d_1 and d values.

Table 2. Mean grain and lath sizes including 95% confidence limits of the mean.

Steel (T_Q)	Prior Austenite Grain Size (PAGS) (μm)	Aspect Ratio	Lath Size (d_1) (μm)	Eff. Grain Size (d) (μm)	$d_{90\%}$ (μm)
Steel A (175 °C)	14.6	1.50	1.28 (± 0.025)	1.61 (± 0.063)	9.27
Steel A (225 °C)	15.0	1.26	1.29 (± 0.026)	1.60 (± 0.059)	8.77
Steel B (175 °C)	14.7	1.33	1.11 (± 0.021)	1.40 (± 0.073)	10.95
Steel B (225 °C)	14.8	1.34	1.32 (± 0.029)	1.63 (± 0.071)	10.59

Li et al. [27] described that packet size and block width (effective grain size) were correlated to PAGS and that the lath width remained approximately the same size. Li et al. [27] showed that an increase of the PAGS, packet size and block width decreased the yield strength of the martensite and effective grain size and directly influenced the toughness, strength, and fatigue crack propagation of lath martensite. In our case, it seems that the composition does not have an effect on the lath size or effective grain size.

3.4. Mechanical Properties

Table 3 presents a summary of the mechanical properties obtained for the TMR-DQP samples. Also included are the corresponding mechanical properties obtained with the DQ versions of the two steels. Tensile test results are the mean values from three samples and the hardness test results are the mean values of 10 measurements on each of three planes, i.e., the L-T plane at the 1/4 thickness depth, the L-N plane and the T-N plane. For ready reference, the retained austenite contents and corresponding carbon contents of different DQ and DQP samples of the two steels are also shown in Table 3. As expected, DQP processing resulted in somewhat lower strengths and hardness values in comparison with the corresponding DQ versions of the two steels. However, steels quenched to $T_Q = 175$ °C showed relatively high strength and hardness values. The 0.2% yield strength ($R_{p0.2}$) was slightly lower than 1100 MPa in one case but, for example, temper rolling should be able to raise the $R_{p0.2}$ to the required level as indicated by the $R_{p1.0}$ values. Both yield and tensile strengths obtained on controlled rolled and DQP processed specimens were lower than those of the DQ versions. The non-proportional percentage of elongation at maximum force (A_g) and the total elongation to fracture (A) were somewhat better at the upper quench stop temperature of 225 °C (5.1%–5.7% and 13.3%–13.6%, respectively) irrespective of the steel type, presumably as a consequence of the higher retained austenite fractions (about 10%) in these DQP samples. Also, the average carbon content of the austenite in these DQP samples was found to be higher, suggesting better stability and thus corroborating higher ductility of these samples. In comparison, the DQ versions too show a small fraction of retained austenite (about 2.6%–2.8%) presumably due to auto-partitioning during quenching. It should be remembered though that the uncertainty of the RA fraction determined using XRD is of the order of ± 1 percentage point. Therefore, the presence of RA in the DQ samples would require confirmation using transmission electron microscopy.

Table 3. Tensile and impact properties obtained with lab rolled steels. Hardness and retained austenite fractions along with their carbon contents are also included in the table for comparison.

Material	T_Q (°C)	$R_{p0.2}$ (MPa)	$R_{p1.0}$ (MPa)	R_m (MPa)	A_g (%)	A (%)
Steel A, DQ	20	1477 ± 110	1918 ± 41	2086 ± 22	3.7 ± 0.3	8.9 ± 1.1
Steel A, DQP	175 *	1322 ± 65	1691 ± 6	1910 ± 30	4.6 ± 0.1	11.9 ± 0.4
Steel A, DQP	225 *	1027 ± 134	1443 ± 80	1717 ± 49	5.7 ± 0.7	13.6 ± 0.6
Steel B, DQ	20	1475 ± 172	1920 ± 57	2095 ± 22	3.9 ± 0.5	10.2 ± 1.5
Steel B, DQP	175 *	1196 ± 175	1626 ± 14	1871 ± 26	4.5 ± 0.5	11.7 ± 2.5
Steel B, DQP	225 *	1108 ± 109	1455 ± 75	1659 ± 35	5.1 ± 0.9	13.3 ± 1.1

Material	T_Q (°C)	KV (−40 °C) (J)	T28J (°C)	HV10	RA (vol%)	RA (C %) **
Steel A, DQ	20	8	>> +40	627 ± 6	2.6	0.43
Steel A, DQP	175 *	38	−80	545 ± 3	6.3	0.60
Steel A, DQP	225 *	43	−92	505 ± 2	10.1	0.65
Steel B, DQ	20	11	>> +40	628 ± 5	2.8	0.47
Steel B, DQP	175 *	45	−105	573 ± 2	6.6	0.61
Steel B, DQP	225 *	41	−73	526 ± 2	10.2	0.94

Tensile properties are averages from three tests. Confidence intervals of 95% are given for the means. $R_{p0.2}$ —proof stress at 0.2% offset strain, $R_{p1.0}$ —proof stress at 1.0% offset strain, R_m —tensile strength, A_g —plastic component of the uniform elongation, A —plastic component of total elongation, KV (−40 °C)—Charpy V impact energy at −40 °C, T28J—transition temperature for an impact energy of 28 J, HV10—Vickers hardness 10 kgf, RA (vol%)—retained austenite proportion, and RA (C%)—carbon content of retained austenite. R_{wp} values of RA measurements were less than 5. * Followed by slow furnace cooling; ** According to Equation (1).

Overall, the mechanical properties of the DQP steels were significantly influenced by the quench stop temperature, even though their difference was only 50 °C, i.e., 175 and 225 °C. In contrast, it seems that the chosen Si, Al and Cr contents had only a small effect on the strength and elongation values for the two examined steel grades.

Interrupted tensile tests were carried out to determine the stability of the RA, i.e., the reduction of the RA content and the mean carbon content of the austenite as a function of strain during room temperature tensile straining for both steels with $T_Q = 225$ °C. Elongations of 2%, 6% and 10% and 2%, 5% and 9.5% were used for steel A and B, respectively. The middle strain values corresponded to the uniform elongations of the two steels, while the highest strains used were between the uniform elongation and the elongation to fracture. XRD measurements revealed that the retained austenite content dropped during straining from 7.5%–8.2% to 0% (see Table 4) before fracture in the case of DQP samples quenched to 225 °C, showing that a large fraction of the original retained austenite transformed during straining. That can result in an early decrease in the instantaneous work hardening exponent (n) and work hardening rate (WHR). A detailed discussion on n and WHR will be presented later in connection with the mechanical properties.

Table 4. Retained austenite fractions along with their average carbon contents from the interrupted tensile test samples.

Steel A	RA (vol%)	RA (C %) *	Steel B	RA (vol%)	RA (C %) *
T_Q 225 °C Base	7.5	0.95	T_Q 225 °C Base	8.2	1.04
T_Q 225 °C 2%	4.3	1.14	T_Q 225 °C 2%	3.8	1.17
T_Q 225 °C 6%	3.0	1.56	T_Q 225 °C 5%	2.3	1.32
T_Q 225 °C 10%	- **	-	T_Q 225 °C 9.5%	- **	-

Base—the undeformed heads, 2–10%—percentage elongation of the tensile test specimens, RA (vol%)—retained austenite proportion, RA (C%)—carbon content of retained austenite. R_{wp} values for the RA measurements were less than 5. * According to Equation (1); ** RA content below the detection limit.

After straining to the uniform elongation values (6% and 5% for steel A and B, respectively), the average carbon content of the untransformed austenite was found to be 1.56% and 1.32% for steel A and B, respectively. These values were 0.95% and 1.04% in undeformed specimens, Table 4. This is to be expected, as the regions of austenite with the highest carbon contents should be the most stable. The content of RA found in the undeformed heads of the tensile specimens, i.e., 7.5%–8.2%,

was lower than that found at the quarter thickness position of the rolled plates, i.e., circa 10% as shown in Figure 3, presumably due to variations in the RA content between different positions in the rolled plates resulting from the unavoidable differences in local rolling and cooling parameters. The same effects can be the cause of the scatter in the tensile and impact test results.

The fraction of RA, carbon content of retained austenite and HV10 hardness plotted against the true strain values for both investigated steels with $T_Q = 225\text{ }^\circ\text{C}$ are presented in Figure 6. The true strains were calculated from the cross-sectional area of the narrowest diameter along the gauge length of each interrupted tensile test sample. The fraction of RA, carbon content of RA and hardness were determined from these cross-sections. Hardness values were the mean of five measurements. As shown in Figure 6a for the investigated DQP variants ($T_Q = 225\text{ }^\circ\text{C}$), it seems that the steel composition has only a slight effect on the rate of decrease of the RA fraction during straining. However, following tensile straining (Figure 6b), the calculated carbon content of the RA was considerably higher for steel A than steel B, indicating that a higher portion of lean interlath austenite must have existed prior to straining but transformed during straining—higher carbon content makes the martensite more stable. As shown in Figure 6c, higher elongation to fracture in steel A leads to higher true strains in the neck and higher hardness values than in steel B.

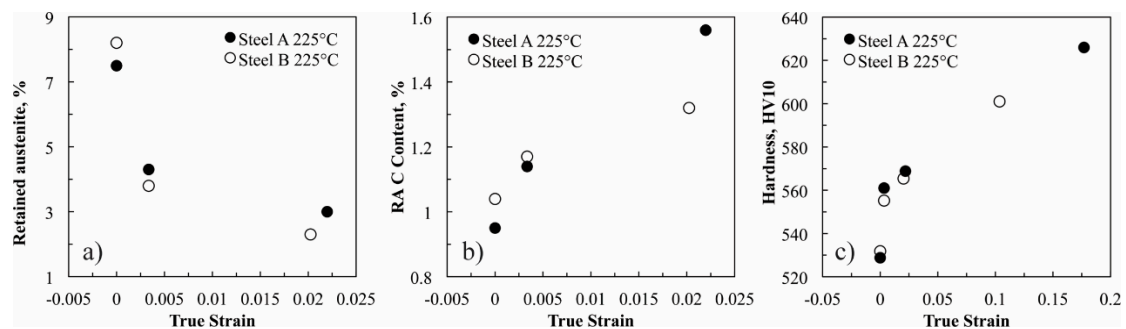


Figure 6. Summary of the effect of true strain on (a) the fraction of retained austenite, (b) the carbon content of retained austenite and (c) the Vickers hardness 10 kgf (HV10) hardness. Note the different strain scale in (c).

Examples of stress–strain curves from testing at room temperature for TMR-DQP processed steels are shown in Figure 7. For comparison, typical tensile measurements of the DQ processed samples are also included. As expected, the highest strengths were reached in the case of DQ processing, whereas the uniform and ultimate elongation were marginally higher for the DQP processed samples at $T_Q = 225\text{ }^\circ\text{C}$. The DQP processed steels have met the yield and tensile strengths $R_{p0.2} \geq 1100\text{ MPa}$ and $R_m \geq 1600\text{ MPa}$, except in the case of the high-Al steel A processed with $T_Q = 225\text{ }^\circ\text{C}$, which showed a lower $R_{p0.2}$ ($1027 \pm 134\text{ MPa}$). In DQ samples, the carbon content of martensite was expected to be higher than that of the DQP materials and the fraction of retained austenite was relatively low (Table 3), which explained the higher strength and hardness of the DQ samples.

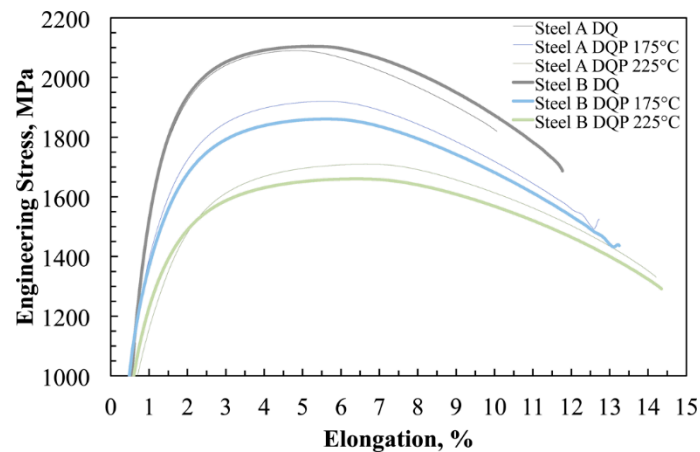


Figure 7. Engineering stress–strain curves of the direct quenched and partitioned (DQP) and direct quenched (DQ) steels.

As stated earlier, there can be some variation in the control of temperature during laboratory DQP processing that can explain the observed variation in the tensile test results. Referring to Figure 7, tensile strengths greater than 1850 and 1650 MPa with total elongations greater than 11.5% and 13% were obtained for both the experimental steels quenched at 175 and 225 °C, respectively. The results show that very high strength can be obtained in combination with reasonable elongation.

True stress–strain curves along with instantaneous work hardening exponents (n) and work hardening rates (WHR) are shown in Figure 8. With $T_Q = 225$ °C, both steels contain higher volume fractions of RA (10%) than the steels processed with $T_Q = 175$ °C (6.3%–6.6%), which is reflected in their higher n values at true strains above 0.03. Of course, it is not only the volume fraction of RA but also the austenite stability that influences the n values. Stability differences can result from the size and shape of the retained austenite pools and interlath films as well as the carbon content distribution in the films and pools, which will depend on the quench stop temperature as evidenced by the different average carbon contents (Table 3). Chiang et al. [28] reported that the carbon content of RA is considered to be the most effective stabilizing factor. Saleh and Priestner [29] described that an increase in the Si content presumably increases the stability of RA. It is believed that an increase in the mechanical stability of the RA raises the value of n . For interrupted quenched 0.15C-1.4Mn dual-phase steels, an increase in the Si content was shown to have increased the value of n as well as the strain to the highest value of n , presumably via an increase in RA stability. However, Saleh and Priestner [29], showed that increasing the Si content beyond 1.44% decreases the maximum value of n and also the strain at which it is achieved. In the present study, the silicon contents of the two steels A and B were 0.5% and 1% respectively, but, in addition, steel A contained 1.1% aluminum. Both steels had approximately the same prior austenite grain size, M_S temperature, volume fraction of RA and almost identical mean carbon contents in the RA. Consequently, the difference in alloying contents with moderately high RA content presumably explains why the values of n and the WHR of steel A were slightly higher than the corresponding values for steel B with $T_Q = 225$ °C (Figure 8). The carbon content of the RA following tensile straining increased in the elongated and necked regions because these were the untransformed austenite films with the highest stability (Table 4). The present results can be compared with those of De Moor et al. [22], reported for a fully austenitized 0.3C-3Mn-1.6Si QP steel, where n values over 0.15 were measured to a strain of 0.14 with a ultimate tensile strength (UTS) of 1520 MPa. For steels A and B, the corresponding strain hardening exponents (n) dropped to low values even before a strain of 0.07 was reached. The XRD measurements showed that most of the RA had transformed before uniform elongation was reached and transformation started already at small elongation values. This suggests that the RA was too unstable, transforming too early to fresh martensite in the straining to have a great effect on uniform elongation.

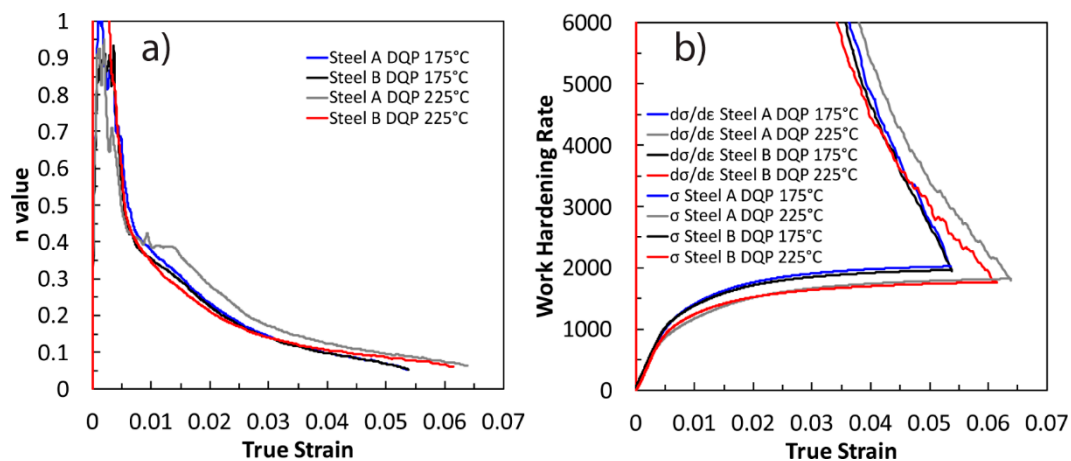


Figure 8. (a) Instantaneous work hardening exponent, (b) work hardening rate and true stress vs. true strain for steel A and B at $T_Q = 175$ and 225 °C.

Comparing the WHRs of DQP processed steel B with $T_Q = 175$ and 225 °C as a function of strain, the WHRs are at the same level up to a true strain of approximately 0.05. Beyond this, the sample with $T_Q = 225$ °C has the higher WHR. Steel A at $T_Q = 225$ °C maintains a higher WHR with increasing strain than steel B. Necking of the tensile specimens with $T_Q = 175$ °C starts earlier than for those with $T_Q = 225$ °C. Though it is not easily visible with the scale used in Figure 8, up to the strain of 0.01, the WHRs of both investigated steels were lower with $T_Q = 225$ °C than with $T_Q = 175$ °C. Compared with the WHRs of the other samples, steel B, with $T_Q = 225$ °C, continued to retain the lowest WHR up to the strain of 0.045, although beyond this strain its WHR began decreasing more slowly. This may be due to the fact that its RA has the highest average carbon content giving it the highest stability.

For QP processed 0.2C-4Mn-1.6Si-1.0Cr steel, Seo et al. [30] showed that the key factors determining the mechanical properties were the kinetics of the martensitic transformation during deformation and the volume fraction of secondary martensite formed during straining. QP processing with low $T_Q = 150$ – 210 °C and $T_P = 450$ °C gave a microstructure comprising carbon enriched RA and carbon depleted tempered primary martensite. With a higher T_Q , above 210 °C, the microstructure also contained carbon enriched, untempered secondary martensite resulting in tension, a higher initial WHR and high UTS, but a decreasing strain level. In the DQP processed variants in the present study there was some secondary martensite formation during the slow furnace cooling to RT but, in addition, at least with a higher $T_Q = 225$ °C, some bainite could form during partitioning. Due to the fact that in the present study the partitioning temperature was not elevated relative to the quench stop temperature, the carbon content of the RA was left lower with the lower $T_P = 175$ °C.

Figure 9 shows the Charpy V impact toughness test results obtained with longitudinal specimens showing the variation of impact energy with the test temperature in the range -120 to 40 °C. DQP treatment considerably improved the impact toughness in comparison with the values obtained with DQ processing. For a given type of microstructure and critical stress of cleavage crack propagation, the 28 J transition temperature was expected to drop as the yield strength decreased. Figure 10 shows that this is indeed the case for the DQP variants when a given quench stop temperature, i.e., volume fraction of RA, was considered.

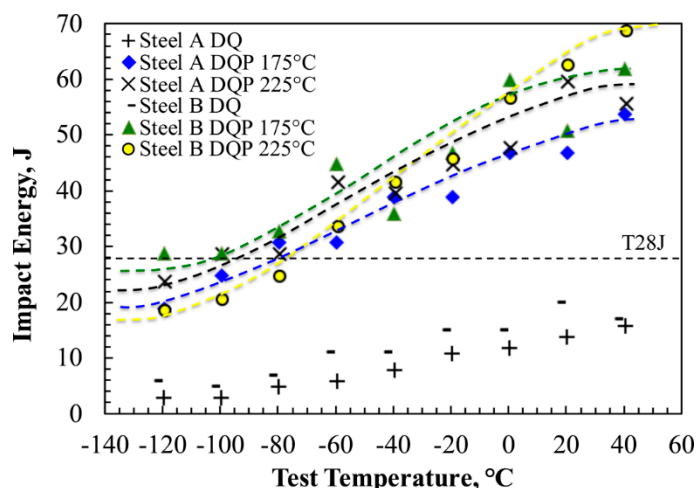


Figure 9. Impact test results for laboratory hot rolled DQ and DQP samples.

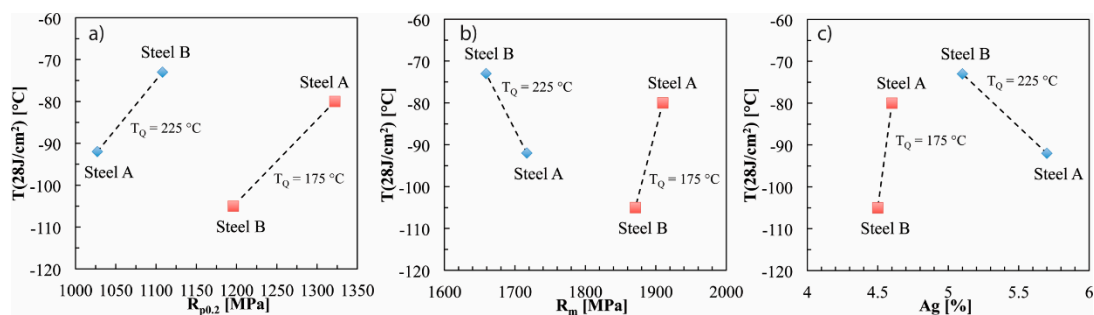


Figure 10. (a) Effect of yield strength ($R_{p0.2}$), (b) tensile strength (R_m) and (c) plastic component of uniform elongation (A_g) on 28 J/cm² transition temperature for DQP processed variants.

What is interesting in Figure 10 is that despite their higher yield stresses, the DQP variants with the lowest volume fraction of RA show similar or better transition temperatures. From a property combination point of view, the best combination of yield strength and 28J transition temperature is obtained for steel B with $T_Q = 175$ °C. The effect of T_Q and steel composition on the relationship between yield strength and transition temperature must be due to microstructural differences that are reflected in differences in the critical stress for cleavage crack nucleation and propagation. This critical stress must be higher in the case of $T_Q = 175$ °C. Looking at the various measured grain sizes shown in Table 2, it seems as though the measures of effective grain size that have been used to rationalize transition temperatures, i.e., d and $d_{90\%}$, are unable to explain the trends in Figure 10. Normally, low-angle grain boundaries are not considered to be effective barriers to cleavage cracks. However, it appears as though the behavior seen in Figure 10 can be partially rationalized in terms of the equivalent circle diameter of sub-grains surrounded by low-angle boundaries, i.e., what we refer to as the lath size. The lath size of the variant with the lowest transition temperature was clearly smaller than that of the other cases. As indicated earlier, most of the retained austenite was finely divided between the laths. This indicates that, the distance between the interlath austenite films has an effect on the transition temperature, with finely divided austenite best assisting in the attainment of a low transition temperature. Figure 10 indicates that it is also better to have a smaller volume fraction of RA (about 6.5%) divided between the laths than a larger fraction (approximately 10%). The reason for this is unclear and will require further investigation, but it might be due to thinner RA films being more stable against transformation to martensite during impact testing. In summary therefore, in the case of the DQP microstructures, contrary to expectations, lath size is probably an important factor controlling the 28 J transition temperatures, due to the presence of interlath austenite.

The test temperature range used was insufficient to determine the upper shelf energies of the various microstructures. However, taking the absorbed energy values at +40 °C as indicative of the trend that would be observed in the upper shelf energies, it can be seen that they correlate with the UTS values associated with the different microstructures (Figure 11), as is commonly found in Charpy V testing.

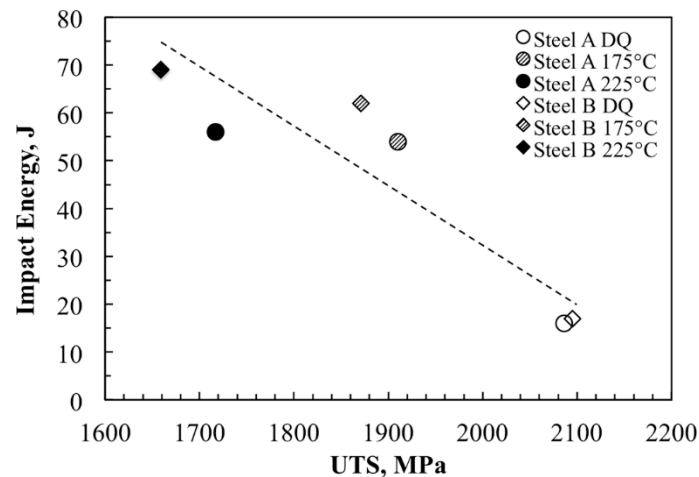


Figure 11. Summary of ultimate tensile strength and the absorbed energy values at +40 °C.

4. Summary and Conclusions

This study encompasses a new TMR-DQP route designed to be appropriate for industrial hot strip production. Two steels (Fe-0.3C-2.0Mn-0.6Si-1.1Al-2.2Cr and Fe-0.3C-1.9Mn-1.0Si-1.0Cr) were laboratory hot rolled, direct quenched and partitioned using the processing parameters derived from preliminary dilatometer measurements on a Gleeble thermomechanical simulator, with theoretical considerations. In order to simulate potential DQP processing on a hot strip mill, partitioning was allowed to occur during slow furnace cooling from the quench stop temperatures (T_Q), which were chosen to be in the M_s – M_f range at 175 and 225 °C. For comparison purposes, the steels were also direct quenched to room temperature, i.e., $T_Q = 20$ °C. The mechanical properties of the final 12 mm thick plates were characterized using hardness, tensile and Charpy V testing. Microstructures were characterized using XRD, LOM, FESEM and EBSD. All the variants comprised lath martensite with varying fractions of retained austenite (RA). The results of the investigation allow the conclusions below to be drawn.

Concerning microstructures, irrespective of the steel chemistry, the fraction of RA increased from 3% to 6.5% to 10% as T_Q increased from 20 through 175 to 225 °C. At the same time, the average carbon content of the RA also increased over the range 0.43 to 0.94 wt%. Almost all of the untransformed austenite present at the quench stop temperature was retained to room temperature. More than 90% of the RA was finely divided as films between the martensite laths and less than 10% as micron-sized pools.

Regarding tensile properties, a TRIP mechanism operated in the TMR-DQP steels with a large fraction of the less stable, carbon-poorer RA transforming to martensite during the course of straining. The result was an improvement in uniformity and total elongations in comparison with DQ microstructures containing little RA.

Regarding impact toughness, the 28 J transition temperature tended to increase with increasing yield stress, but, for a given yield stress, it was lowered by the presence of thin interlath layers of RA, such that a small volume fraction of RA was divided between fine spaced laths produces the lowest transition temperature. At higher temperatures, towards the upper shelf, impact toughness was increasingly controlled by tensile strength, with the highest absorbed energies associated with the lowest strengths.

The overall best combination of properties was obtained with the Fe-03C-1.9Mn-1.0Si-1.0Cr composition, thermomechanically rolled and quenched to 175 °C followed by furnace cooling to room temperature: yield strength ($R_{p0.2}$) = 1200 MPa, tensile strength = 1870 MPa, plastic component of uniform elongation = 4.5%, elongation to fracture = 12%, and 28 J Charpy V transition temperature = −105 °C. However, the research shows that the practical implementation of DQP processing on a hot strip mill with either of the current compositions may be challenging due to the sensitivity of the mechanical properties to the quench stop temperature.

Author Contributions: Supervision, M.S.; writing—original draft, P.K.; writing—review and editing, A.K., O.H., D.P. and J.K.

Funding: This research was funded by RFCS, grant agreement RFSR-CT-2014-00019.

Acknowledgments: This work was carried out within the auspices of the SUPERHIGH program of the Research Fund Coal and Steels (RFCS). We would like to thank the staff of the Research Center of SSAB Europe Oy Raahе for their valuable cooperation.

Conflicts of Interest: The authors declare no conflicts of interest.

References

1. di Schino, A.; Alleva, L.; Guagnelli, M. Microstructure Evolution during Quenching and Tempering of Martensite in a Medium C Steel. *Mater. Sci. Forum* **2012**, *715–716*, 860–865. [[CrossRef](#)]
2. Yan, S.; Liu, X.; Liu, W.J.; Lan, H.; Wu, H. Comparison on mechanical properties and microstructure of a C-Mn-Si steel treated by quenching and partitioning (Q&P) and quenching and tempering (Q&T) processes. *Mater. Sci. Eng. A* **2014**, *620*, 58–66.
3. Speer, J.; Matlock, D.K.; De Cooman, B.C.; Schroth, J.G. Carbon partitioning into austenite after martensite transformation. *Acta Mater.* **2003**, *51*, 2611–2622. [[CrossRef](#)]
4. Santofimia, M.J.; Nguyen-Minh, T.; Zhao, L.; Petrov, R.; Sabirov, I.; Sietsma, J. New low carbon Q&P steels containing film-like intercritical ferrite. *Mater. Sci. Eng. A* **2010**, *527*, 6429–6439.
5. Thomas, G.A.; Speer, J.G.; Matlock, D.K. Quenched and partitioned microstructures produced via Gleeble simulations of hot-strip mill cooling practices. *Metall. Mater. Trans. A Phys. Metall. Mater. Sci.* **2011**, *42*, 3652–3659. [[CrossRef](#)]
6. Arlazarov, A.; Ollat, M.; Masse, J.P.; Bouzat, M. Influence of partitioning on mechanical behavior of Q&P steels. *Mater. Sci. Eng. A* **2016**, *661*, 79–86.
7. Wang, L.; Speer, J.G. Quenching and Partitioning Steel Heat Treatment. *Metallogr. Microstruct. Anal.* **2013**, *2*, 268–281. [[CrossRef](#)]
8. Somani, M.C.; Porter, D.A.; Karjalainen, L.P.; Suikkanen, P.P.; Misra, R.D.K. Process design for tough ductile martensitic steels through direct quenching and partitioning. *Mater. Today Proc.* **2015**, *2*, S631–S634. [[CrossRef](#)]
9. Vanderschueren, D.; De Meyer, M.; De Cooman, B.C.; Wor, K.E.Y. The influence of the substitution of Si by Al on the Properties of Cold Rolled C-Mn-Si TRIP Steels. *ISIJ Int.* **1999**, *39*, 813–822.
10. Speer, J.G.; De Moor, E.; Findley, K.O.; Matlock, D.K.; De Cooman, B.C.; Edmonds, D.V. Analysis of Microstructure Evolution in Quenching and Partitioning Automotive Sheet Steel. *Metall. Mater. Trans. A* **2011**, *42*, 3591–3601. [[CrossRef](#)]
11. De Moor, E.; Lacroix, S.; Samek, L.; Penning, J.; Speer, J.G. Dilatometric Study of the Quench and Partitioning Process. In Proceedings of the 3rd International Conference on Advanced Structural Steels, Gyeongju, Korea, 22–24 August 2006.
12. Tsukatani, I.; Hashimoto, S.; Inoue, T. Effects of Silicon and Manganese Addition on Mechanical Properties of High-Strength Hot-Rolled Sheet Steel Containing Retained Austenite. *ISIJ Int.* **1991**, *31*, 992–1000. [[CrossRef](#)]
13. di Schino, A.; Braccisi, C.; Cianetti, F.; di Nunzio, P.E.; Mengaroni, S.; Calvillo, P.R.; Cabrera, J.M. Manganese Effect on Q&P CMnSi Steels. *Mater. Sci. Forum* **2016**, *879*, 430–435.
14. Somani, M.C.; Porter, D.A.; Karjalainen, L.P.; Misra, R.D.K. On Various Aspects of Decomposition of Austenite in a High-Silicon Steel during Quenching and Partitioning. *Metall. Mater. Trans. A Phys. Metall. Mater. Sci.* **2014**, *45*, 1247–1257. [[CrossRef](#)]

15. Li, Y.-J.; Li, X.-L.; Yuan, G.; Kang, J.; Chen, D.; Wang, G.-D. Microstructure and partitioning behavior characteristics in low carbon steels treated by hot-rolling direct quenching and dynamical partitioning processes. *Mater. Charact.* **2016**, *121*, 157–165. [[CrossRef](#)]
16. Tan, X.; Xu, Y.; Yang, X.; Liu, Z.; Wu, D. Effect of partitioning procedure on microstructure and mechanical properties of a hot-rolled directly quenched and partitioned steel. *Mater. Sci. Eng. A* **2014**, *594*, 149–160. [[CrossRef](#)]
17. Dyson, D.J.; Holmes, B. Effect of alloying additions on the lattice parameter of austenite. *J. Iron Steel Inst.* **1970**, *208*, 469–474.
18. Van Dijk, N.H.; Butt, A.M.; Zhao, L.; Sietsma, J.; Offerman, S.E.; Wright, J.P.; Van Der Zwaag, S. Thermal stability of retained austenite in TRIP steels studied by synchrotron X-ray diffraction during cooling. *Acta Mater.* **2005**, *53*, 5439–5447. [[CrossRef](#)]
19. Scott, C.P.; Drillet, J. A study of the carbon distribution in retained austenite. *Scr. Mater.* **2007**, *56*, 489–492. [[CrossRef](#)]
20. Koistinen, D.P.; Marburger, R.E. A general equation prescribing the extent of the austenite-martensite transformation in pure iron-carbon alloys and plain carbon steels. *Acta Metall.* **1959**, *7*, 59–60. [[CrossRef](#)]
21. van Bohemen, S.M.C.; Sietsma, J. Martensite formation in partially and fully austenitic plain carbon steels. *Metall. Mater. Trans. A Phys. Metall. Mater. Sci.* **2009**, *40*, 1059–1068. [[CrossRef](#)]
22. De Moor, E.; Speer, J.G.; Matlock, D.K.; Kwak, J.-H.; Lee, S.-B. Effect of Carbon and Manganese on the Quenching and Partitioning Response of CMnSi Steels. *ISIJ Int.* **2011**, *51*, 137–144. [[CrossRef](#)]
23. Maheswari, N.; Chowdhury, S.G.; Kumar, K.C.H.; Sankaran, S. Influence of alloying elements on the microstructure evolution and mechanical properties in quenched and partitioned steels. *Mater. Sci. Eng. A* **2014**, *600*, 12–20. [[CrossRef](#)]
24. Edmonds, D.V.; He, K.; Rizzo, F.C.; De Cooman, B.C.; Matlock, D.K.; Speer, J.G. Quenching and partitioning martensite—A novel steel heat treatment. *Mater. Sci. Eng. A* **2006**, *438–440*, 25–34. [[CrossRef](#)]
25. Kajjalainen, A.J.; Suikkanen, P.P.; Limnell, T.J.; Karjalainen, L.P.; Kömi, J.I.; Porter, D.A. Effect of austenite grain structure on the strength and toughness of direct-quenched martensite. *J. Alloys Compd.* **2013**, *577*, S642–S648. [[CrossRef](#)]
26. Hannula, J.; Kömi, J.; Porter, D.A.; Somani, M.C.; Kajjalainen, A.; Suikkanen, P.; Yang, J.R.; Tsai, S.P. Effect of Boron on the Strength and Toughness of Direct-Quenched Low-Carbon Niobium Bearing Ultra-High-Strength Martensitic Steel. *Metall. Mater. Trans. A Phys. Metall. Mater. Sci.* **2017**, *48*, 5344–5356. [[CrossRef](#)]
27. Li, S.; Zhu, G.; Kang, Y. Effect of substructure on mechanical properties and fracture behavior of lath martensite in 0.1C-1.1Si-1.7Mn steel. *J. Alloys Compd.* **2016**, *675*, 104–115. [[CrossRef](#)]
28. Chiang, J.; Lawrence, B.; Boyd, J.D.; Pilkey, A.K. Effect of microstructure on retained austenite stability and work hardening of TRIP steels. *Mater. Sci. Eng. A* **2011**, *528*, 4516–4521. [[CrossRef](#)]
29. Saleh, M.H.; Priestner, R. Retained austenite in dual-phase silicon steels and its effect on mechanical properties. *J. Mater. Process. Technol.* **2001**, *113*, 587–593. [[CrossRef](#)]
30. Seo, E.J.; Cho, L.; Estrin, Y.; De Cooman, B.C. Microstructure-mechanical properties relationships for quenching and partitioning (Q&P) processed steel. *Acta Mater.* **2016**, *113*, 124–139.

